Magesh Kumar, K. K. and Kumar, M. and Yuan, T. and Sheng, Z. M. and Chen, M. (2015) Terahertz radiation from plasma filament generated by two-color laser gas–plasma interaction. Laser and Particle Beams, 33 (03). pp. 473-479. ISSN 1469-803X , http://dx.doi.org/10.1017/S0263034615000518

Terahertz radiation from plasma filament generated by two-color laser gas plasma interaction

Magesh Kumar K K[1]*, Manoj Kumar[2], Yuan Tao[1], Z. M. Sheng[1,3] and M. Chen[1]†

[1] *Key Laboratory for Laser Plasmas, Shanghai Jiao Tong University, Shanghai 200240, China*

[2] *Center for Quantum-Beam-based Radiation Research, KAERI, Daejeon 305-353, Korea*

[3] *SUPA, Department of Physics, University of Strathclyde, Glasgow G4 0NG, UK*

April 15, 2015

Abstract

We develop a theoretical model for THz radiation generation, when an intense short laser pulse (ω_1, k_1) is mixed with its frequency shifted second harmonic (ω_2, k_2), where $\omega_2 = 2\omega_1 + \omega_T$ and ω_T is in the THz range in plasma. The lasers exert a ponderomotive force on the electrons and drive density perturbations at ($2\omega_1$, $2k_1$) and ($\omega_2 - \omega_1$, $k_2 - k_1$). These density perturbations couple with the oscillatory velocities of the electron due to the lasers and produce a nonlinear current at ($\omega_2 - 2\omega_1$, $k_2 - 2k_1$). This current acts as an antenna to produce the THz radiation. The Terahertz power depends upon the square of plasma density and $I_1^2 I_2$, where I_1 and I_2 are the intensities of fundamental and second harmonic laser. The radiation is mainly along the forward direction. Two dimensional particle in cell simulations are used to study the near field radiation properties.

*Electronic mail : mageshkumar2006@gmail.com

†Electronic mail : minchen@sjtu.edu.cn

1 Introduction

Terahertz radiation generation has attracted a lot of attention in recent years because of its potential applications in imaging (Jackson et al., 2008; Jackson et al., 2011), remote sensing (Antonsen et al., 2007), chemical and security identification (Shen et al., 2005). From the view of generation mechanisms, several different theories have already been proposed such as four-wave-mixing (Cook & Hochstrasser., 2000; Xie et al., 2006), mode conversion (Sheng et al., 2005), transient current model (Kress et al., 2004; Kim et al., 2007; Chen et al., 2012; Wu et al., 2008; Li et al., 2012) and quantum mechanical model (Karpowicz & Zhang, 2009). And from the view of experimental and theoretical studies, THz radiation can come from one-color (Amico et al., 2007; Wu et al., 2011; Tzortzakis et al., 2002; Matsubara et al., 2012; Zhao et al., 2014; Chen et al., 2007; Sprangle et al., 2004; Hu et al., 2010) and two-color (Peñano et al., 2010; Yang & Du, 2013; Zhong et al., 2006; Oh et al., 2013; Zhao et al., 2013; Wang et al., 2011; Wang et al., 2011; You et al., 2012; Varshney et al., 2014; Varshney et al., 2013; Varshney et al., 2013) laser gas interactions. These filaments generation and THz radiation have gained special attention due to the relative simplicity of the experimental operation.

THz radiation from one-color laser gas interaction has been studied by various groups. Amico *et al.* (Amico et al., 2007) have reported the emission of strongly collimated THz beam in forward direction from plasma filament and Tzortzakis *et al.* (Tzortzakis et al., 2002) have observed the emission of THz radiation from plasma filament in the direction perpendicular to the laser propagation axis. Peñano *et al.* (Penano et al., 2010) have given a detailed analysis of THz emission from plasma filament. They found that in the spatially modulated medium the ponderomotive force has superluminal Fourier components which is responsible for the THz emission.

Similarly, for two-color laser gas interaction, Cook and Hochstrasser (Cook & Hochstrasser., 2000) first reported their THz emission experimental results. They have noted that the four-wave mixing due to third order nonlinearity in air is responsible for THz generation. Oh *et al.* (Oh et al., 2013) have studied THz generation from gaseous and clustered plasma. Their experimental observations confirm scalable THz generation with increasing filament length. Similarly You *et al.* (You et al., 2012) have observed phase matched THz generation from two color laser and obtained considerable increase in yield with filament length. Matsubara *et al.* (Matsubara et al., 2012) have reported ultra-broadband radiation up to 200 THz via two-color laser mixing. Other possible mechanisms have also been proposed to explain the THz generation from two color laser gas interaction. Transient photocurrent model developed by Kim *et al.* (Kim et al., 2007), use symmetry-broken laser field to excite coherent THz emission from air. Klarskov *et al.* (Klarskov et al., 2013) have studied three dimensional intensity profile emitted from a two-color air plasma. They have reported that the nonlinear optical response of the plasma and the transient photocurrents result in emission of a conical beam of THz radiation.

In this paper we propose and discuss another possible mechanism for THz radiation generation via two-color laser pulses interaction in a collisional plasma. The physical mechanism of THz generation is different from the above two-color transient photocurrent model. In our case, the THz generation current is not due to ionization induced electrons' residual momentum, however, it is due to the electric current generated by the ponderomotive force of the two color beat wave in plasma. The THz generation process is as follows: An intense short laser pulse with frequency ω_1 and wave number k_1 is mixed with its frequency shifted second harmonic with frequency ω_2 and wave number k_2, where $\omega_2 = 2\omega_1 + \omega_T$, ω_T is in the THz range, in plasma. The lasers exert a ponderomotive force on the electrons and drive density perturbations at $(2\omega_1, 2k_1)$ and $(\omega_2 - \omega_1, k_2 - k_1)$.

These density perturbations couple with the oscillatory velocities of the electron due to the lasers and produce a nonlinear current density at $(\omega_2 - 2\omega_1,\, k_2 - 2k_1)$ and generate the p-polarized electromagnetic wave radiation. The paper is organized as follows: In section II and III we calculate the nonlinear current density including the collisional effects and obtain far field THz emission. In section IV, two dimensional particle in cell (2D-PIC) simulation is carried out to study the near field radiation properties and the conclusion is given in section V.

2 Nonlinear Current Density

As shown in Fig. 1, we consider two-color pulse propagation in plasma with frequency ω_1 and wave vector $\vec{k}_1$, represented by the field

$$\vec{E}_1 = \hat{x}\mathrm{A}_{10} e^{-r^2/2R_0^2} e^{-i(\omega_1 t - k_1 z)}, \tag{1}$$

and its frequency shifted second harmonic of frequency ω_2 and wave vector $\vec{k}_2$,

$$\vec{E}_2 = \hat{x}\mathrm{A}_{20} e^{-r^2/2R_0^2} e^{-i(\omega_2 t - k_2 z)}, \tag{2}$$

where, $\omega_2 = 2\omega_1 + \omega_T$, ω_T is in the THz range in plasma, $k_1 = (\omega_1/c)\sqrt{1-\omega_p^2/\omega_1^2}$, $k_2 = (\omega_2/c)\sqrt{1-\omega_p^2/\omega_2^2}$, $\omega_p = \sqrt{n_0 e^2/m\epsilon_0}$ is the plasma frequency, n_0 is the electron density and R_0 is the initial laser spot size. $-e$ and m are the charge and mass of electron respectively. The polarization of the lasers are kept same (x axis) to obtain maximum current density.

Using the equation of motion, $(\partial/\partial t + \nu)\vec{v} = -\frac{e}{m}\vec{E}$, the oscillatory velocities of electrons due to the lasers are obtained as,

$$\vec{v}_{\omega_1} = \frac{e\vec{E}_1}{mi\omega_1(1 + i\nu/\omega_1)}, \tag{3}$$

$$\vec{v}_{\omega_2} = \frac{e\vec{E}_2}{mi\omega_2(1 + i\nu/\omega_2)}, \tag{4}$$

where ν is the collision frequency.

The ponderomotive force exerted on the electrons at $(2\omega_1, 2k_1)$ and $(\Delta\omega, \Delta k)$ are,

$$\vec{F}_{P_{(2\omega_1)}} = -e\vec{v}_{\omega_1} \times \vec{B}_{\omega_1} = -\frac{e^2 k_1 E_1^2}{2mi\omega_1^2(1 + i\nu/\omega_1)}\hat{z}, \tag{5}$$

$$\begin{aligned} \vec{F}_{P_{\Delta\omega}} =& -e(\vec{v}_{\omega_2} \times \vec{B}^*_{\omega_1} + \vec{v}^*_{\omega_1} \times \vec{B}_{\omega_2}) \\ =& \frac{e^2 \Delta k(\vec{E}_2.\vec{E}^*_1)}{2mi\omega_1\omega_2}(1 + i\nu/\varpi)\hat{z}, \end{aligned} \tag{6}$$

where $\varpi = \frac{\omega_1\omega_2\Delta k}{\omega_2 k_2 + \omega_1 k_1}$, $\Delta\omega = \omega_2 - \omega_1$ and $\Delta k = k_2 - k_1$.

The oscillatory velocity of the electrons at $(2\omega_1, 2k_1)$ due to the ponderomotive force $\vec{F}_{P_{2\omega_1}} (= e\nabla\phi_{p(2\omega_1)})$ and self consistent field $(\vec{E}_{2\omega_1} = -\nabla\phi_{s(2\omega_1)})$, is on solving the equation of motion,

$$(\partial/\partial t + \nu)\vec{v}_{2\omega_1} = \frac{e}{m}\nabla(\phi_{s(2\omega_1)} + \phi_{p(2\omega_1)}), \tag{7}$$

turns out to be,

$$\vec{v}_{2\omega_1} = -\frac{e\nabla(\phi_{s(2\omega_1)} + \phi_{p(2\omega_1)})}{2im\omega_1(1 + i\nu/2\omega_1)}, \tag{8}$$

where $\phi_{p(2\omega_1)} = eE_1^2/4m\omega_1^2(1+i\nu/\omega_1)$. The velocity $\vec{v}_{2\omega_1}$, gives rise to density oscillation at frequency $(2\omega_1)$, which on solving the equation of continuity $\frac{\partial}{\partial t}n_{2\omega_1} + \nabla\cdot(n_0\vec{v}_{2\omega_1}) = 0$, turns out to be,

$$n_{2\omega_1} = \frac{n_0 e\nabla^2(\phi_{s(2\omega_1)} + \phi_{p(2\omega_1)})}{4\omega_1^2 m(1+i\nu/2\omega_1)}. \tag{9}$$

Substituting Eq. (9) in Poisson's equation, $\nabla^2\phi_{s(2\omega_1)} = n_{2\omega_1}e/\epsilon_0$, one obtains, $\phi_{s(2\omega_1)} = (\omega_p^2/4\omega_1^2)/(1+i\nu/2\omega_1 - \omega_p^2/4\omega_1^2)\phi_{p(2\omega_1)}$. Hence the perturbed velocity and density modifies to,

$$\vec{v}_{2\omega_1} = -\frac{e^2k_1E_1^2}{4m^2\omega_1^3}\frac{1}{(1+i\nu/\omega_1)[1+i\nu/2\omega_1 - (\omega_p^2/4\omega_1^2)]}\hat{z}, \tag{10}$$

$$n_{2\omega_1} = -\frac{n_0e^2k_1^2E_1^2}{4m^2\omega_1^4}\frac{1}{(1+i\nu/\omega_1)[1+i\nu/2\omega_1 - (\omega_p^2/4\omega_1^2)]}. \tag{11}$$

Similarly the ponderomotive force $\vec{F}_{P_{\Delta\omega}}$ gives rise to oscillatory velocity to the electrons $\vec{v}_{(\Delta\omega,\Delta k)}$ and drives the density perturbation

$$n_{(\Delta\omega,\,\Delta k)} = \frac{n_0e^2\Delta k^2(\vec{E}_2.\vec{E}_1^*)}{2m^2\omega_1\omega_2\Delta\omega^2}\frac{(1+i\nu/\varpi)}{(1+i\nu/\Delta\omega - \omega_p^2/\Delta\omega^2)}. \tag{12}$$

Hence the total nonlinear current density at $[\omega_T(=\omega_2-2\omega_1)\ ,\ k_T(=k_2-2k_1)]$ is

$$\begin{aligned}\vec{J}^{NL}_{(\omega,k)} =& -\frac{e}{2}n^*_{2\omega_1}\vec{v}_{\omega_2} - \frac{e}{2}n_{\Delta\omega}\vec{v}^*_{\omega_1} \\ =& J_0e^{-3r^2/2R_0^2}e^{-i(\omega_Tt-k_Tz)}\hat{x},\end{aligned} \tag{13}$$

where $J_0 = -i\frac{n_0ec}{8}a_{20}a_{10}^2(1+i\nu/\omega_1)\,(\alpha_1+i\alpha_2)$, $a_{10} = eA_{10}/m\omega_1c$, $a_{20} = eA_{20}/m\omega_2c$,

$\alpha_1 = \frac{k_1^2c^2/\omega_1^2}{(1-\omega_p^2/4\omega_1^2)}\frac{(1-\omega_p^2/4\omega_1^2)^2}{(1-\omega_p^2/4\omega_1^2)^2+\nu^2/4\omega_1^2}\left[1+\frac{\nu^2}{2\omega_1\omega_2(1-\omega_p^2/4\omega_1^2)}\right] +$
$2\big(\frac{\Delta kc}{\Delta\omega}\big)^2\frac{1}{(1-\omega_p^2/\Delta\omega^2)}\left[1+\frac{\nu^2}{\Delta\omega\varpi(1-\omega_p^2/\Delta\omega^2)}\frac{(1-\omega_p^2/\Delta\omega^2)^2}{(1-\omega_p^2/\Delta\omega^2)^2+\nu^2/\Delta\omega^2}\right]$, and

$$\alpha_2 = \frac{\nu}{\omega_1}[\frac{k_1^2c^2/\omega_1^2}{(1-\omega_p^2/4\omega_1^2)}(\frac{1}{2(1-\omega_p^2/4\omega_1^2)}+\frac{\omega_1}{\omega_2})\frac{(1-\omega_p^2/4\omega_1^2)^2}{(1-\omega_p^2/4\omega_1^2)^2+\nu^2/4\omega_1^2}+$$

$$2(\frac{\Delta kc}{\Delta\omega})^2\frac{\omega_1/\varpi}{(1-\omega_p^2/\Delta\omega^2)}(1-\frac{\varpi}{\Delta\omega(1-\omega_p^2/\Delta\omega^2)}\frac{(1-\omega_p^2/\Delta\omega^2)^2}{(1-\omega_p^2/\Delta\omega^2)^2+\nu^2/\Delta\omega^2})].$$

If one takes, $\nu/\omega_1 << 1$, Eq. (13) reduces to,

$$\vec{J} = -i\frac{n_0ec}{8}a_{20}a_{10}^2\alpha_1e^{-3r^2/2R_0^2}e^{-i(\omega_Tt-k_Tz)}\hat{x}, \tag{14}$$

where $\alpha_1 = \frac{k_1^2c^2/\omega_1^2}{(1-\omega_p^2/4\omega_1^2)} + 2\big(\frac{\Delta kc}{\Delta\omega}\big)^2\frac{1}{(1-\omega_p^2/\Delta\omega^2)}$.

The two terms in the above Eq. is due of the density fluctuations at $2\omega_1$ and $\Delta\omega = \omega_2 - \omega_1$ respectively.

3 Terahertz Generation as an Antenna

The retarded vector potential at a far point $\vec{r}(r,\theta,z)$ due to the current density in the filament of length L and radius r_f is given as,

$$\vec{A}(r,\,t) = \frac{\mu_0}{4\pi}\int\frac{\vec{J}(r',\,t-R/c)}{R}d^3V', \tag{15}$$

where $R = |r-r^{'}|$ and the volume integral is over the entire length and cross-section of the filament. As the filament radius is less than the THz wavelength, ponderomotive force driven current can be taken to be

unmodified by the self field and the nonlinear current source can be treated like a wire antenna as far as the radiation field is concerned. Hence, for the filament of radius $r_f << c/\omega_T$, the nonlinear current density can be written as,

$$\vec{J}^{NL} = J_0 e^{-3r'^2/2R_0^2} e^{-i(\omega_T(t-r/c)-\omega_T z'(1+\frac{3\omega_p}{4\omega_1}-\cos\theta)/c)}\hat{x}, \tag{16}$$

where $k_T(= k_2 - 2k_1) \approx \frac{\omega_T}{c}(1+\frac{3\omega_p}{4\omega_1})$ and $R \approx r - z^{'}\cos\theta$ are used. Here θ is the angle between r and z axis (Fig. 1). Using Eq.(17) in (16), one gets,

$$\vec{A}(r,\,t) = \hat{x}\frac{\mu_0 J_0 e^{-i\omega_T(t-r/c)}}{4\pi}\int_0^L\int_0^{2\pi}\int_0^{r_f}\frac{e^{-3\rho'^2/2R_0^2}e^{i(1+\frac{3\omega_p}{4\omega_1}-\cos\theta)\omega_T z'/c}}{r - z'\cos\theta}\rho' d\rho' d\phi' dz'. \tag{17}$$

Hence the vector potential at larger distance becomes,

$$\vec{A}(r,\,t) = \hat{x}\frac{\mu_0 J_0 r_f^2 e^{-i\omega_T(t-r/c)}}{4r}\frac{[e^{i(1+\frac{3\omega_p}{4\omega_1}-\cos\theta)\omega_T L/c}-1]}{i\omega_T(1+\frac{3\omega_p}{4\omega_1}-\cos\theta)/c}. \tag{18}$$

The term $3\omega_p/4\omega_1$ inside the parenthesis in Eq .(19) can be neglected for filaments of length $L << \frac{2\omega_1}{3\omega_p}\frac{\lambda_{\rm THz}}{\pi}$, where $\lambda_{\rm THz}$ is the wavelength of THz radiation. For typical parameters, $\omega_1/\omega_p \sim 100$, $\lambda_{\rm THz} \sim 100\mu m$, the filament length $L << 2mm$.

Therefore, for far field, the magnetic field and electric field of the THz wave is,

$$\begin{aligned}
\vec{B} =& \nabla\times\vec{A} \simeq (i\omega_T/c)\hat{r}\times\vec{A} = (\hat{r}\times\hat{x})\frac{\mu_0 r_f^2 J_0 e^{-i\omega_T(t-r/c)}}{4r}\frac{[e^{i(1-\cos\theta)\omega_T L/c}-1]}{(1-\cos\theta)}, \\
\vec{E} =& -\partial\vec{A}/\partial t = -i\omega_T\vec{A} = \hat{x}\frac{\mu_0 c r_f^2 J_0 e^{-i\omega_T(t-r/c)}}{4r}\frac{[e^{i(1-\cos\theta)\omega_T L/c}-1]}{(1-\cos\theta)}.
\end{aligned} \tag{19}$$

Hence the time averaged Poynting's vector,

$$\vec{S}_{av} = \hat{r}\frac{c}{2\mu_0}|B|^2 \simeq \hat{r}\frac{\mu_0 c r_f^4 |J_0|^2}{8r^2}\frac{\sin^2[(1-\cos\theta)\omega_T L/2c]}{(1-\cos\theta)^2}(1-\sin^2\theta\cos^2\phi). \tag{20}$$

The above Eq. represents the angular distribution of the radiated THz energy. One may note that as θ decreases the THz power increases and attains maximum around $\theta = 0$. For $\phi = \pi/2$, $\theta \sim 0$ the maximum power of the radiated field in the forward direction turns out to be

$$\frac{\vec{S}_{av} r^2}{P_1} = \hat{r} S_0 \left(\frac{\omega_T L}{2c}\right)^2. \tag{21}$$

Normalizing the THz power by peak power of laser, $P_1 = \frac{\pi R_0^2}{2\mu_0 c}|A_{10}|^2$, Eq. (21) becomes

$$\frac{\vec{S}_{av} r^2}{P_1} = \hat{r} S_0 \frac{\sin^2[(1-\cos\theta)\omega_T L/2c]}{(1-\cos\theta)^2}(1-\sin^2\theta\cos^2\phi), \tag{22}$$

where $S_0 = \frac{1}{4\pi}\frac{a_{10}^2 a_{20}^2}{64}\left(\frac{\omega_p r_f}{c}\right)^2\left(\frac{r_f}{R_0}\right)^2\left(\frac{\omega_p}{\omega_1}\right)^2(1+\nu^2/\omega_1^2)(\alpha_1^2+\alpha_2^2)$.

Hence the normalized total THz power can be written as,

$$\frac{P_{\rm THz}}{P_1} = \int_0^{2\pi}\int_0^{\pi}(\vec{S}_{av} r^2/P_1)\sin\theta d\theta d\phi. \tag{23}$$

4 Particle-in-Cell Simulation and Discussion

OSIRIS code (Fonseca et al., 2002) has been used to carry out the 2D-PIC simulation to trace the THz field inside and outside the plasma filament of finite length and radius. The length (L) and radius (r_f) of the plasma column used for the simulation is $1mm \times 16\mu m$. We here consider a fully ionized plasma column of density $n_0 = 10^{17} cm^{-3}$. Corresponding plasma frequency is $\omega_p = 1.77 \times 10^{13}$ rad/sec. The lasers are linearly polarized ($\hat{x}$) and propagate in the $+z$ direction. The frequencies of the lasers are taken as $\omega_1 = 2.355 \times 10^{15}$ rad/sec and $\omega_2 = 4.722 \times 10^{15}$ rad/sec, such that the difference frequency $\omega_T = (\omega_2 - 2\omega_1) = 1.2 \times 10^{13}$ rad/sec, lies in the THz range. Corresponding laser wavelengths are λ_1=800nm, λ_2=399nm and the peak intensities $I_1 = I_2 = 2 \times 10^{14} W/cm^2$, with the normalized field amplitudes $a_{10} = 0.01$ and $a_{20} = 0.005$. The pulse has a gaussian temporal shape with $T = 150t_0$ and the spot sizes $r_0 = 6.4\mu m$, where $t_0 = 2\pi/\omega_1$ is the laser period. The cell size is $0.025 \times 0.1\mu m^2$ and the time step interval is 0.03fs. The total simulation time is $900t_0$. In the PIC simulation, the collisional effect has been neglected. Our result only show the short term and near field distribution of the THz radiation.

We have traced the electric field of THz radiation close to the laser axis and at distances larger than the filament spot size ($r_f = 6.4\mu m$). Fixing z at $z = 400\lambda_1$ we recorded the THz field in the $+x$ direction. The electric field spectrum of THz wave inside and outside of the plasma filament is plotted in Fig. 2. The solid lines represent THz field inside the filament and the broken lines represent the field outside. The THz spectrum inside and outside the plasma filament are different but carries quite interesting details. Inside the plasma filament, one can see two prominent maximas, corresponding to $\omega/\omega_1 = 0.0037 = \omega_p/2\omega_1$ i.e, $\omega = \omega_p/2$ and $\omega/\omega_1 = 0.0075 = \omega_p/\Delta\omega$ i.e, $\omega = \omega_p$. The minima between these frequencies is at $\omega/\omega_1 = 0.005 = \omega_T/\omega_1$ i.e, $\omega = \omega_T$, corresponding $f = \omega_T/2\pi = 2$THz. This is because the lasers exert ponderomotive force on electrons at frequency $2\omega_1$ and at beat frequency $\Delta\omega$. The ponderomotive force together with the self consistent field, gives rise to density perturbations at $2\omega_1$ and $\Delta\omega$ (cf. the denominator part of Eqs. 11 and 12). These density perturbations drive a nonlinear current at $\omega_T = \omega_2 - 2\omega_1$ (cf. Eq .13) and generate the p-polarized electromagnetic wave radiation. Thus the two maximas appearing in the spectrum are due to the two terms in nonlinear current J_x. As one moves out of the filament, the aforementioned maximas decrease and disappear at $x = 2.5r_f$, as shown in Fig. 2, giving rise to a single maxima around $\omega = 0.005\omega_1 = \omega_T$. One may also note that the field amplitude decreases steadily with increase in distance x within the filament, and outside, the amplitude decreases rapidly with distance and the spectrum broadens as well.

From Eq. (20), we obtain the angular distribution of the far field THz wave. As the angle $\theta \sim 0$, one gets from Eq .(20) the on-axis THz field strength, $E = \frac{n_0 e r_f^2}{16\epsilon_0 r} \frac{\omega_T L}{2c} a_{20} a_{10}^2$. The electric field of the THz is proportional to plasma density n_0, square of filament radius r_f, the filament length L and inverse of distance r. To validate the efficacy of our analytical calculation we compare the profile of THz field (From Eq. (20)) with the experimental results of Zhong *et al.* (Zhong et al., 2006). Zhong *et al.* (Zhong et al., 2006) have investigated the THz radiation emission via four wave mixing in air plasma and have observed highly directional THz waves with a divergence angle smaller than 10^o. For our analytical calculation we used plasma density $n_0 = 10^{17} cm^{-3}$. Fig. 3 shows the angular distribution of THz field at a distance $r = 1m$, plotted for the filament lengths $L =$ 3.9mm (black), 8.9mm(blue), 13mm(red) and 35mm(green). We have used the same filament lengths obtained by Zhong *et al.* (Zhong et al., 2006). One may note that the THz field amplitude attains maximum at $\theta = 0$ and

falls rapidly with increasing angle. This means that the radiation emission is largely contained in the forward direction. With an eight fold increase in the filament length, the THz field profile gets strongly modified and becomes highly directional with a divergence angle less than 10^o. Hence it clearly indicates that our analytical result in Fig. 3 is comparable with the experimental results of Zhong *et al.* (Zhong et al., 2006).

We would now compare the angular distribution of the THz yield with the experimental results of Gorodetsky *et al.* (Gorodetsky et al., 2014). Gorodetsky *et al.* (Gorodetsky et al., 2014) have proposed a model to explain the conical behavior of the THz emission from the two-color laser induced plasma filaments. Their studies show that for a nonuniform plasma filament the conical angle remains constant with the filament length, while the angle decreases with length for uniform plasma. In our case we have considered a uniform plasma filament as mentioned before. Fig. 4 shows the angular distribution of the normalized THz yield for the filament lengths $L = 2.8$mm (black), 10.5mm (blue) and 17.7mm (red). Here we used the filament lengths of Gorodetsky *et al.* (Gorodetsky et al., 2014) for the comparative study. The THz power is null along the laser axis ($\theta = 0$) and attains maxima between the angles $\theta = 2\sin^{-1}(\sqrt{\frac{N}{L\omega_T/c}})$, where $N = \pi, 2\pi, 3\pi ... n\pi$. Therefore larger the filament length L, smaller will be the emission cone angle. Fig. 5 shows the variation of conical angle with the filament length. The half angular width calculated from the above expression can reproduce the experimental results of Gorodetsky *et al.* (Gorodetsky et al., 2014). For example, the half angular width of the first strongest maxima (for $N = \pi$) for $L = 10.5$mm turns out to be $\theta_{1/2} = 5^o$, which agrees well with the experimental results of Gorodetsky *et al.* (Gorodetsky et al., 2014).

Finally we compare analytically calculated yield (P_{THz}/P_1) with the experimental results obtained by Oh *et al.* (Oh et al., 2013). Oh *et al.* (Oh et al., 2013) have studied high power THz radiation generation via two color laser filamentation and have achieved filament lengths varying from few centimeters to 1.5m by increasing the input laser energy. Hence for a filament of length $L = 1m$, the half angular width of the first strongest emission cone turns out to be 0.5^o and corresponding yield $P_{\mathrm{THz}}/P_1 = 1.6 \times 10^{-5}$, which is comparable to the estimation of Oh *et al.* (Oh et al., 2013).

5 conclusion

In conclusion, we have studied four wave mixing process for THz radiation generation when two-color laser pulses propagate in plasma. The THz field amplitude scales with laser intensity as $I_1\sqrt{I_2}$ and proportional to plasma density n_0. The polarization of the lasers are kept same to enhance the emission of THz radiation. The lasers drive a nonlinear current at ω and generate the p-polarized electromagnetic wave radiation. Using 2D-PIC simulations we analyzed the spectrum of THz field both inside and outside the plasma filament. Inside the filament the spectrum showed two prominent maximas at $\omega_p/2\omega_1$ and $\omega_p/\Delta\omega$ supporting our analytical framework. These maximas merge together to form a single maxima around $\omega_T/2\pi = 2$THz outside the filament. The field amplitude decreases steadily with increase in distance x within the filament, and outside, the amplitude decreases rapidly with distance and the spectrum broadens as well.

From the angular distribution of the THz field profile, the radiation emission is found to be largely contained in the forward direction. The THz power and amplitude are found to be very sensitive to the filament length. Hence the THz power can be increased by increasing the filament length, also by using more laser power. The analytically calculated THz field amplitude and yield are found to be in agreement with the previous studies. The

THz radiation intensities from such mechanism is far lower than the photon ionization current mechanism where ionization current dominates radiation. However, this mechanism does not depend on ionization current which usually results from residual ionization momentum, the radiation current here is excited by the ponderomotive force of the two color beat wave. For an existed fully ionized gas plasma, the former photon ionization current generation mechanism does not work, the current model still works. However the radiated THz field should be smaller with several orders of magnitude. At the same time, in our model, some basic THz radiation characters are the same as other models, such as the radiation intensity dependence on the two color intensities and angular distributions. To get a correct explanation of THz generation mechanism in an experiment, careful studies should be made by comparing more aspects of radiation characters.

6 Acknowledgement

This work was supported by the National Basic Research Program of China (Grant Nos. 2013CBA01504 and 2014CB339801), and the National Science Foundation of China (Grant Nos. 11121504, 11374209, and 11374210). M.C. appreciates supports from Shanghai Science and Technology Commission (Grant No. 13PJ1403600). Simulations were performed on the Supercomputer PI at Shanghai Jiao Tong University. The authors would like to acknowledge the OSIRIS Consortium, consisting of UCLA and IST (Lisbon, Portugal) for the use of OSIRIS. MK appreciates the useful discussions with Feiyu Li.

References

ANTONSEN, T. M., JOHN PALASTRO & MILCHBERG, H. M. (2007). Excitation of Terahertz radiation by laser pulses in nonuniform plasma channels. *Phys. Plasmas* **14**, 033107-033115.

CHEN, M., PUKHOV, A., PENG, X. -YU. & WILLI, O. (2008). Theoretical analysis and simulations of strong Terahertz radiation from the interaction of ultrashort laser pulses with gases. *Phys. Rev. E* **78**, 046406-046412 ; CHEN, M., YUAN, X.H., SHENG, Z.M. (2012). Scalable control of Terahertz radiation from ultrashort laser-gas interaction. *Appl. Phys. Lett.* **101**, 161908-161911 .

CHEN, Y., THE′BERGE, F., KOSAREVA, O., PANOV, N., KANDIDOV, V. P. & CHIN, S. L. (2007). Evolution and termination of a femtosecond laser filament in air. *Opt. Lett.* **32**, 3477-3479.

COOK, D. J. & HOCHSTRASSER, R. M . (2000). Intense Terahertz pulses by four-wave rectification in air. *Opt. Lett.* **25**, 1210-1212.

D'AMICO, C., HOUARD, A., FRANCO, M., PRADE, B., MYSYROWICZ, A., COUAIRON, A. & TIKHONCHUK, V. T. (2007). Conical forward THz emission from femtosecond-laser-beam filamentation in air . *Phys. Rev. Lett.* **98**, 235002-235005.

FONSECA, R. A., SILVA, L. O., TSUNG, F. S., DECYK, V. K., LU, W., REN, C., MORI, W. B., DENG, S., LEE, S., KATSOULEAS, T. & ADAM, J. C. (2002). OSIRIS: A three-dimensional, fully relativistic particle in cell code for modeling plasma based accelerators. *Lect. Notes Comput. Sci.* **2331**,342-351.

GORODETSKY, A., KOULOUKLIDIS, A. D., MASSAOUTI, M. & TZORTZAKIS, S. (2014). Physics of the conical broadband terahertz emission from two-color laser-induced plasma filaments. *Phys. Rev. A* **89**, 033838-033843.

HU,G. Y., SHEN, B., LEI, A.L., LI, R. X. & XU, Z. Z. (2010).Transition-Cherenkov radiation of terahertz generated by super-luminous ionization front in femtosecond laser filament. *Laser and Part. Beams* **28**, 399-407.

JACKSON, J. B., BOWEN, J., WALKER, G., LABAUNE, J., MOUROU, G., MENU, M. & FUKUNAGA, K. (2011). A survey of terahertz applications in cultural heritage Conservation science. *IEEE Trans. Terahertz Sci. and Tech.*. **1**, 220-231.

JACKSON, J.B., MOUROU, M., WHITAKER, J.F., DULING III, I.N., WILLIAMSON, S.L., MENU, M. & MOUROU, G.A. (2008). Terahertz imaging for non-destructive evaluation of mural paintings. *Opt. Comm.* **281**, 527-532.

KARPOWICZ, N. & ZHANG, X. -C. (2009). Coherent Terahertz echo of tunnel ionization in gases. *Phys. Rev. Lett.* **102**, 093001-093004.

KIM, K. Y., GLOWNIA, J. H., TAYLOR, A. J. & RODRIGUEZ, G. (2007). Terahertz emission from ultrafast ionizing air in symmetry-broken laser fields. *Opt. Express* **15**, 4577-4584.

KLARSKOV, P., STRIKWERDA, A. C., IWASZCZUK K. & JEPSEN, P. U. (2013). Experimental three-dimensional beam profiling and modeling of a terahertz beam generated from a two-color air plasma. *New J. Phys.* **15**, 075012-075024.

KRESS, M., LÖFFLER, T., EDEN, S., THOMSON, M. & ROSKOS, H. G. (2004). Terahertz-pulse generation by photoionization of air with laser pulses composed of both fundamental and second-harmonic waves. *Opt. Lett.* **29**, 1120-1122.

LI, Y. T., LI, C., ZHOU, M. L., WANG, W. M., DU, F., DING, W. J., LIN, X. X., LIU, F., SHENG, Z. M.,

PENG, X. Y., CHEN, L. M., MA, J. L., LU, X., WANG, Z. H., WEI, Z. Y. & ZHANG, J. (2012). Strong terahertz radiation from relativistic laser interaction with solid density plasmas. *Appl. Phys. Lett.* **100**, 254101-254104.

MATSUBARA, E., NAGAI, M. & ASHIDA, M. (2012). Ultrabroadband coherent electric field from far infrared to 200 THz using air plasma induced by 10 fs pulses. *Appl. Phys. Lett.* **101**, 011105-011108.

OH, T. I., YOU, Y. S., JHAJJ, N., ROSENTHAL, E. W., MILCHBERG H. M. & KIM, K. Y. (2013). Intense terahertz generation in two-color laser filamentation: energy scaling with terawatt laser systems. *New J. Phys.* **15**, 075002-075018.

PEÑANO, J. R., SPRANGLE, P., HAFIZI, B., GORDON, D. & SERAFIM, P. (2010). Terahertz generation in plasmas using two-color laser pulses. *Phy. Rev. E* **81**, 026407-026414.

VARSHNEY, P., SAJAL, V., CHAUHAN, P., KUMAR, R. & SHARMA, N. K. (2014). Effects of transverse static electric field on terahertz radiation generation by beating of two transversely modulated Gaussian laser beams in a plasma. *Laser Part. Beams* **32**, 375-381.

VARSHNEY, P., SAJAL,V., BALIYAN, S., SHARMA, N. K., CHAUHAN, P. & KUMAR, R. (2013). Strong terahertz radiation generation by beating of two x-mode spatial triangular lasers in magnetized plasma. *Laser Part. Beams* **33**, 51-58.

VARSHNEY, P., SAJAL, V., SINGH, K. P., KUMAR, R. & SHARMA,N. K. (2013). Strong terahertz radiation generation by beating of extra-ordinary mode lasers in a rippled density magnetized plasma. *Laser Part. Beams* **31**, 337-344.

SHEN, Y. C., LO, T., TADAY, P. F., COLE, B. E., TRIBE, W. R. & KEMP, M. C. (2005). Detection and identification of explosives using Terahertz pulsed spectroscopic imaging. *Appl. Phys. Lett.* **86**, 241116 -241118.

SHENG, Z.M., MIMA, K., ZHANG, J. & SANUKI, H. (2005). Emission of electromagnetic pulses from laser wakefields through linear mode conversion. *Phys. Rev. Lett.* **94**, 095003-095006.

SPRANGLE, P., PEÑANO, J. R., HAFIZI, B. & KAPETANAKOS, C. A. (2004). Ultrashort laser pulses and electromagnetic pulse generation in air and on dielectric surfaces. *Phys. Rev. E* **69**, 066415-66432.

TZORTZAKIS, S., MÉCHAIN, G., PATALANO, G., ANDRE′, Y.-B., PRADE, B., FRANCO, M., & MYSYROWICZ, A., MUNIER, J.-M., GHEUDIN, M., BEAUDIN, G., & ENCRENAZ, P. (2002). Coherent subterahertz radiation from femtosecond infrared filaments in air. *Opt. Lett.* **27**, 1944-1946.

WANG, T. J., DAIGLE, J. F., YUAN, S., THE′BERGE, F., CHÂTEAUNEUF, M., DUBOIS, J., ROY, G., ZENG, H. & CHIN, S. L. (2011). Remote generation of high-energy terahertz pulses from two-color femtosecond laser filamentation in air. *Phys. Rev. A* **83**, 053801-053804.

WANG, W. M., TONG LI, Y., SHENG, Z. M., LU, X. & ZHANG, J. (2013). Terahertz radiation by two-color lasers due to the field ionization of gases. *Phys. Rev. E* **87**, 033108-033117.

WU, H. -C., MEYER-TER-VEHN, J. & SHENG, Z. -M. (2008). Phase-sensitive terahertz emission from gas targets irradiated by few-cycle laser pulses. *New. J.Phys.* **10**, 043001-043010.

WU, H.-C., MEYER-TER-VEHN, J., RUHL, H. & SHENG, Z.-M. (2011). Terahertz radiation from a laser plasma filament. *Phys. Rev. E* **83**, 036407-036410.

XIE, X., DAI, J. & ZHANG, X. C. (2006). Coherent control of THz wave generation in ambient air. *Phys. Rev. Lett.* **96**, 075005-075008.

YANG, N. & DU, H. (2013). Terahertz emission and energy reservoir of air- plasma filamentation induced by

two-color femtosecond laser pulses. *Optics Comm.* **297**, 118-120.

YOU, Y. S., OH, T. I. & KIM, K.Y. (2012). Off-Axis Phase-Matched Terahertz Emission from Two-Color Laser-Induced Plasma Filaments. *Phys. Rev. Lett.* **109**, 183902-183906.

ZHAO, J., CHU, W., GUO, L., WANG, Z., YANG, J., LIU, W., CHENG, Y. & XU, Z. (2013). Terahertz imaging with sub-wavelength resolution by femtosecond laser filament in air. *Nat. Sci. Reports* **4**, 3880-3886.

ZHAO, J., ZHANG, Y., WANG, Z., CHU, W., ZENG, B., LIU, W., CHENG, & XU, Y. Z. (2014). Propagation of terahertz wave inside femtosecond laser filament in air. *Laser Phys. Lett.* **11**, 095302-095307.

ZHONG, H., KARPOWICZ, N. & ZHANG, X. -C. (2006). Terahertz emission profile from laser-induced air plasma. *Appl. Phys. Lett.* **88**, 261103-261105.

Figure Caption

1. Schematic of THz radiation when two color laser pulses propagate in air plasma.

2. The electric field spectrum of THz wave inside and outside of the plasma filament. The solid lines represent the THz field inside the filament and the broken lines represent the field outside.

3. Variation of normalized THz field $|E|^2$ (arb.units) with angle θ for the filament lengths $L = 3.9$mm (black), 8.9mm(blue), 13mm(red) and 35mm(green).

4. Variation of normalized THz yield (arb.units) with angle θ for the filament lengths $L = 2.8$mm (black), 10.5mm (blue) and 17.7mm (red).

5. Variation of conical angle with filament length.

Click here to download Figure: fig1.docx

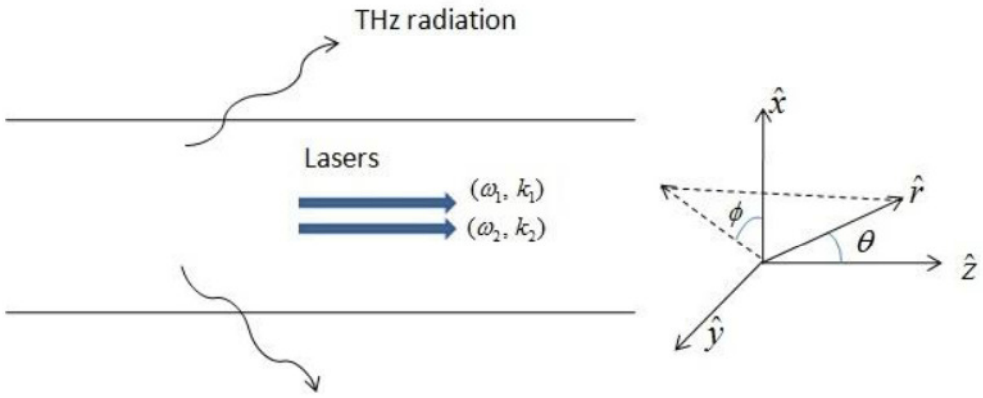

Figure 1

Click here to download Figure: fig2.docx

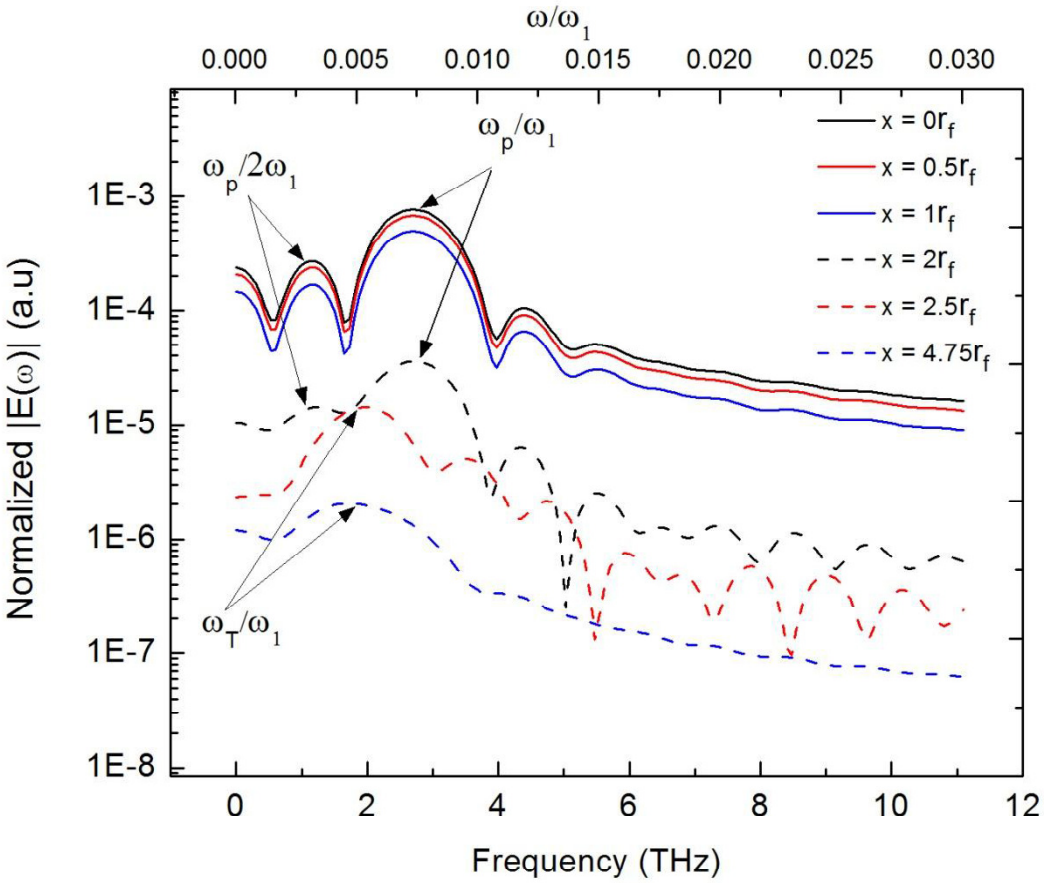

Figure 2

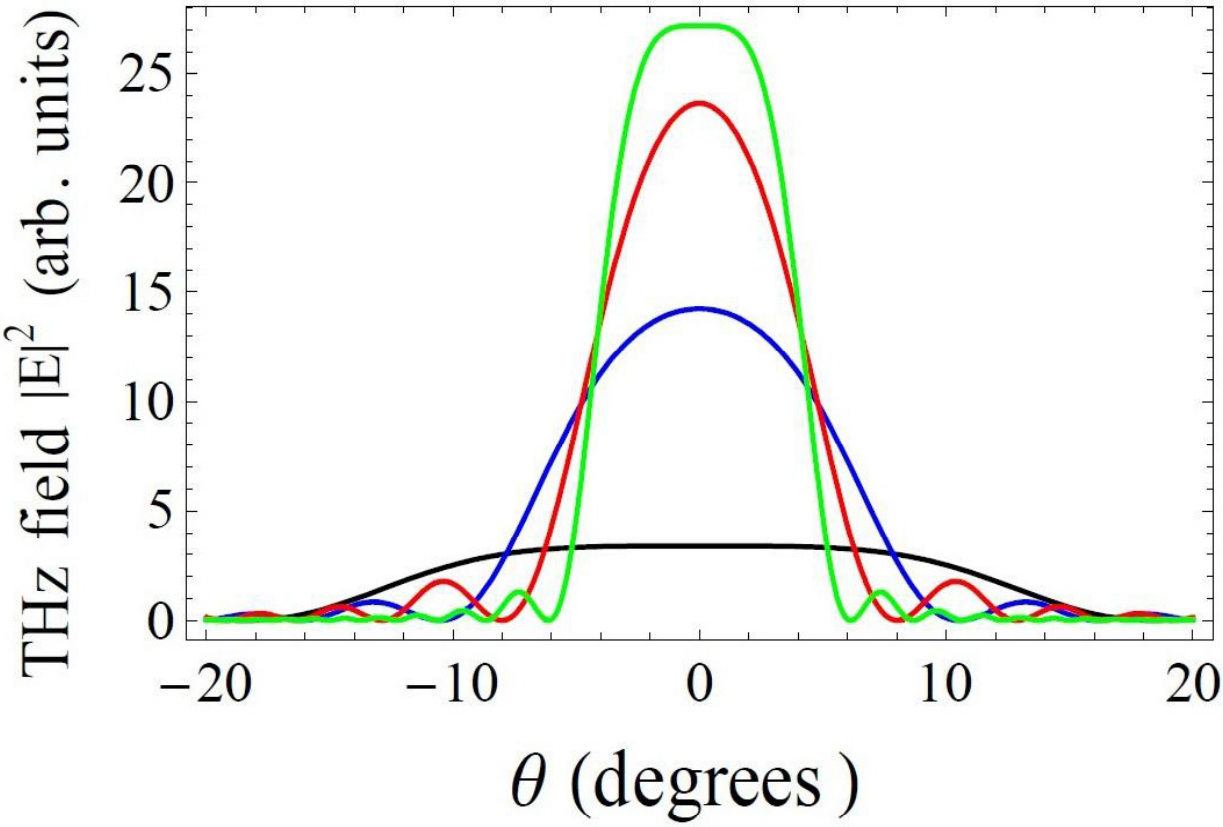

Figure 3

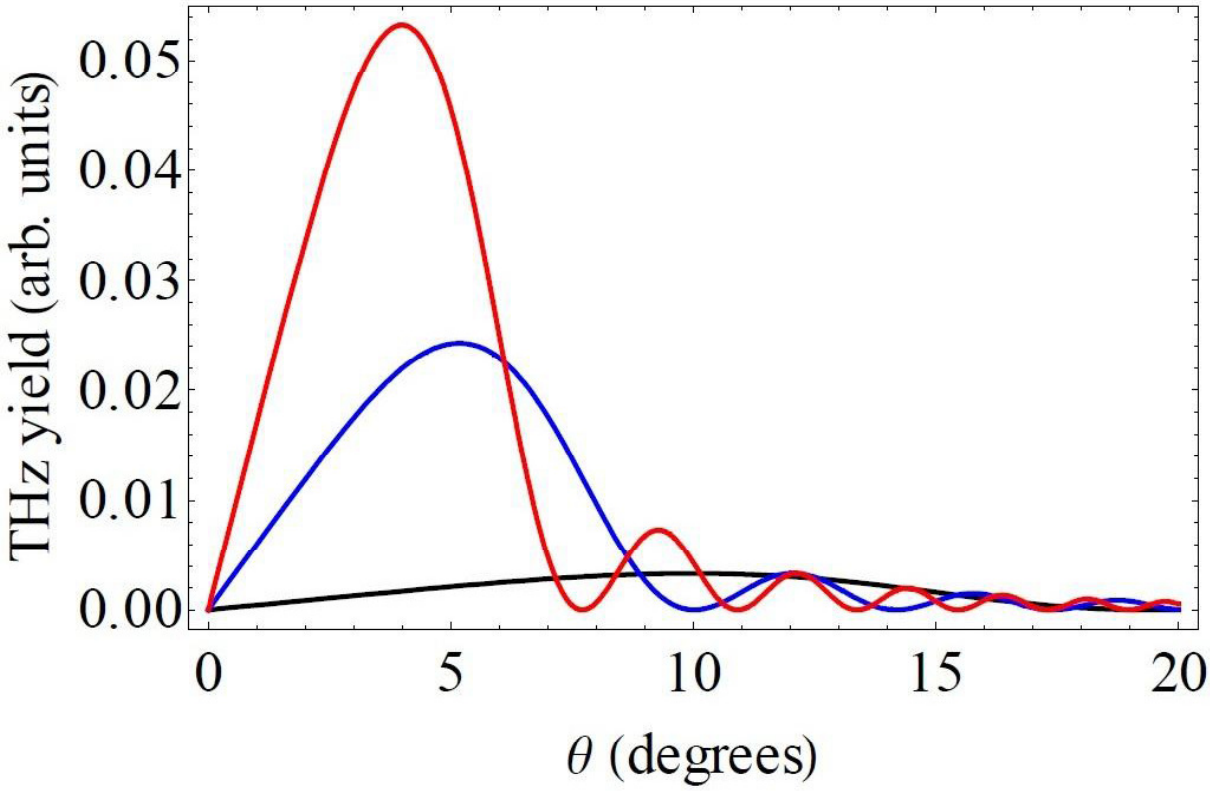

Figure 4

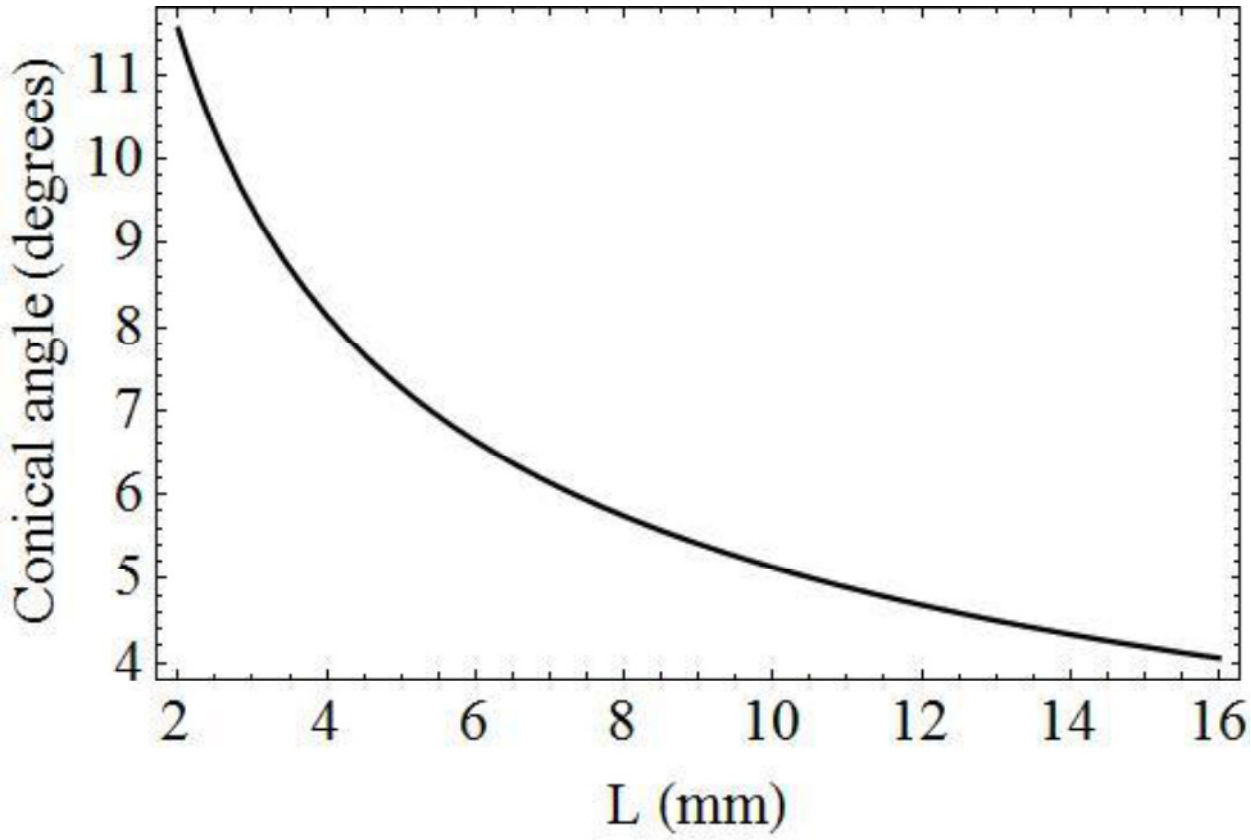

Figure 5